All-electrical monitoring of bacterial antibiotic susceptibility in a microfluidic device

Yichao Yang[a,b], Kalpana Gupta[c,d], and Kamil L. Ekinci[a,b,1]

[a]Department of Mechanical Engineering, Division of Materials Science and Engineering, Boston University, Boston, MA 02215; [b]Photonics Center, Boston University, Boston, MA 02215; [c]Department of Medicine, Section of Infectious Diseases, Veterans Affairs Boston Healthcare System, Boston, MA 02132; and [d]Department of Medicine, Boston University School of Medicine, Boston, MA 02118

Edited by David A. Weitz, Harvard University, Cambridge, MA, and approved March 26, 2020 (received for review December 17, 2019)

The lack of rapid antibiotic susceptibility tests adversely affects the treatment of bacterial infections and contributes to increased prevalence of multidrug-resistant bacteria. Here, we describe an all-electrical approach that allows for ultrasensitive measurement of growth signals from only tens of bacteria in a microfluidic device. Our device is essentially a set of microfluidic channels, each with a nanoconstriction at one end and cross-sectional dimensions close to that of a single bacterium. Flowing a liquid bacteria sample (e.g., urine) through the microchannels rapidly traps the bacteria in the device, allowing for subsequent incubation in drugs. We measure the electrical resistance of the microchannels, which increases (or decreases) in proportion to the number of bacteria in the microchannels. The method and device allow for rapid antibiotic susceptibility tests in about 2 h. Further, the short-time fluctuations in the electrical resistance during an antibiotic susceptibility test are correlated with the morphological changes of bacteria caused by the antibiotic. In contrast to other electrical approaches, the underlying geometric blockage effect provides a robust and sensitive signal, which is straightforward to interpret without electrical models. The approach also obviates the need for a high-resolution microscope and other complex equipment, making it potentially usable in resource-limited settings.

antibiotic susceptibility testing | growth and morphology | antibiotic resistance | microfluidics

Multidrug-resistant bacteria pose an increasingly serious threat to global public health (1). While drug resistance in bacteria occurs naturally due to random genetic mutations and genetic exchanges between strains and species, it is accelerated partly because of inappropriate antibiotic use (2). Strategies, such as rapid point-of-care antibiotic susceptibility testing, can facilitate targeted antibiotic treatments and impede the spread of antibiotic resistance (3–5). However, standard antibiotic susceptibility tests (ASTs) suffer from a lengthy cell culture step and take 24 h to 48 h to complete (6, 7). Given the risks associated with delayed therapy, physicians typically have little choice but to empirically prescribe broad-spectrum antibiotics while waiting for the microbiological analysis (8, 9). The development of rapid ASTs would improve morbidity and mortality and could help reduce the prevalence of multidrug-resistant bacteria (10).

The "gold standard" ASTs are phenotypic and measure the growth of bacteria in the presence of antibiotics on solid agar plates or in liquid solutions. After incubation for 24 h to 48 h, the susceptibility of the bacterial strain can be determined from the growth size and patterns on the agar plate or the optical density of the liquid solution (4). Polymerase chain reaction (PCR) provides the quintessential genotypic AST (11). PCR directly detects the resistance gene(s) from a very small bacteria sample and hence is quite rapid. However, it still has limited utility, because only a few resistance genes are firmly associated with phenotypic antibiotic resistance, and newly acquired resistance mechanisms may not be detectable (12).

Given the limitations of mainstay ASTs, there is a significant push for developing novel methods that can inform on bacterial resistance at early stages of cell growth. These novel and emerging ASTs typically employ microfluidics and microdevices, because these devices allow for effective sample use and are sensitive to small signals (13). State-of-the-art approaches isolating bacteria in nanodroplets (14, 15), on microbeads (16), inside microfluidic channels (17–21), and on and inside micromechanical resonators (22) have all allowed testing on a few cells and even single cells. These approaches involve a variety of transduction mechanisms to access the response of bacteria to antibiotics, including high-resolution imaging (14, 15, 17, 18) and mechanical (16, 22), impedance (19), and electrochemical sensing (20, 21). More recently, high-resolution imaging of growth of bacteria trapped in microchannels (17, 18) has allowed for ASTs in under an hour (17). While ingenious, each method comes with some drawbacks (23), and it remains to be seen whether or not any will achieve sufficient robustness needed for routine clinical practice.

Our method and device build on the positive attributes of recent approaches and address some of their shortcomings. As in earlier work (17, 18), we trap and incubate cells in a microfluidic channel; our measurement, however, is entirely electrical. The effect underlying the bacterial growth signal in our device is simple geometric blockage: As bacteria grow (or die) in the microchannel, the channel resistance to electrical current increases (decreases). The change in the number of bacteria in the device, therefore, is directly proportional to the measured resistance change, and is available without fits to multiparameter circuit models (24). The device can directly be used with

Significance

For the past 50 y, antibiotics have cured common bacterial infections quickly and effectively. Many strains of bacteria, however, are gaining resistance to common antibiotics. The solution to this problem includes a more judicious use of antibiotic therapies, directed by rapid point-of-care antibiotic susceptibility tests. The focus here is a simple all-electrical sensing approach implemented in a microfluidic device that measures the growth of a tiny bacteria sample in antibiotics. This approach has the potential to rapidly provide antibiotic susceptibility of bacteria along with minimum inhibitory concentrations and inform of the mechanisms of action of antibiotics—all without resorting to high-resolution microscopy.

Author contributions: Y.Y., K.G., and K.L.E. designed research; Y.Y. performed research; Y.Y. and K.L.E. analyzed data; and Y.Y. and K.L.E. wrote the paper.

Competing interest statement: K.L.E. discloses a potential of conflict of interest, as he is the cofounder of a company, which aims to commercialize this technology. No potential conflicts of interest exist for Y.Y. and K.G.

This article is a PNAS Direct Submission.

[1]To whom correspondence may be addressed. Email: ekinci@bu.edu.

This article contains supporting information online at https://www.pnas.org/lookup/suppl/doi:10.1073/pnas.1922172117/-/DCSupplemental.

First published April 29, 2020.

urine and probably other bodily fluids, provided that the fluids contain ions. Another interesting and useful attribute of the approach is that it provides electrical clues on how bacteria respond to antibiotics. We observe different short-time fluctuation patterns in electrical signals coming from bacteria incubated in bacteriostatic and bactericidal antibiotics, suggesting that morphological changes are also encoded into the electrical signals. In cases where both growth and morphological analysis are required, this unique feature may be useful (25–27). We reemphasize that microscopy is not required in our approach; at the current stage of development, it is used only as a validation tool.

Results

Device Design and Loading. The design and basic principle of operation of the microfluidic device is shown in Fig. 1. The device is essentially a continuous polydimethylsiloxane (PDMS) channel on a glass substrate with thin metal film electrodes. At the center, the channel tapers down into 10 smaller microchannels, each with linear dimensions $l \times w \times h \approx 100 \times 2 \times 2\ \mu m^3$. On one end of each of these parallel microchannels, a physical constriction ($l \times w \times h \approx 5 \times 0.8 \times 2\ \mu m^3$) is fabricated for trapping bacteria from a flowing sample (Fig. 1*B*). During operation, a pressure-driven flow of a bacteria solution is established through the microchannels from the inlet to the outlet (Fig. 1 *A* and *B*). The bacteria in the solution cannot pass through the constriction and are trapped as shown in the optical microscope image in Fig. 1*B*. In the experiments, the electrical resistance of the microchannel region is monitored using a four-wire measurement (Fig. 1*B*). When the microchannels are filled with just media with no bacteria, that is, empty, their typical resistances are $R_{em} \approx 3\ M\Omega \pm 30\ k\Omega$.

At the start of each experiment, the bacteria sample is loaded into the microfluidic device from the inlet by keeping the inlet at a pressure ~ 10 kPa above the outlet. Fig. 1*C* shows the number of trapped cells as a function of time for *Klebsiella pneumoniae* suspensions at different bacteria concentrations in the range from 5×10^3 CFU/mL to 2×10^7 CFU/mL. Approximately 60 bacteria are captured in ~ 30 min at 5×10^5 CFU/mL, which is close to the cell density in the urine of a urinary tract infection (UTI) patient (28). At the most dilute bacteria concentration (5×10^3), we only trapped a few bacteria over the 30-min period. The trapping efficiency at low concentration could be improved by increasing Δp or the number of microchannels.

Fig. 1 *C*, *Inset* shows the electrical signal, as bacteria number increases in the microchannels. Here, we show the resistance increase ΔR from the empty state, as a function of the number n of bacteria in the microchannels from three separate experiments using different microchannels with identical nominal linear dimensions. The increase in ΔR with n can be understood in simple terms. The microchannel filled with the media is essentially an electrical conductor, due to the ions in the buffer. The bacteria in the microchannel "clog" the microchannel and reduce the effective cross-section, thereby increasing the resistance. The data follow a linear trend, with a resistance change of $\Delta R_1^{(KP)} \approx 2.5 \pm 0.3\ k\Omega$ per bacterium (*K. pneumoniae*) added. Similar experiments (*SI Appendix*, Fig. S3) give $\Delta R_1^{(EC)} \approx 3.7 \pm 0.3\ k\Omega$ and $\Delta R_1^{(SS)} \approx 3.5 \pm 1.1\ k\Omega$ for *Escherichia coli* and *Staphylococcus saprophyticus*, respectively. An estimate using simple geometric arguments for *K. pneumoniae* provides $\Delta R_1 \approx 1.5\ k\Omega$, not far from the measured value (*SI Appendix*, *Supplemental Materials and Methods*). These ΔR_1 values provide a good calibration for the experiments and allow us to estimate that ~ 20 cells are needed to perform a conclusive AST, due to the long-term electrical drifts.

Since we do not use very high pressures during loading, bacteria occasionally accumulate at other locations in the device, particularly at lithographical edges and at the entrances of microchannels. When this happens, the measured resistances correspond to larger bacteria numbers than are counted from microscope image. The electrical signal is quite robust against

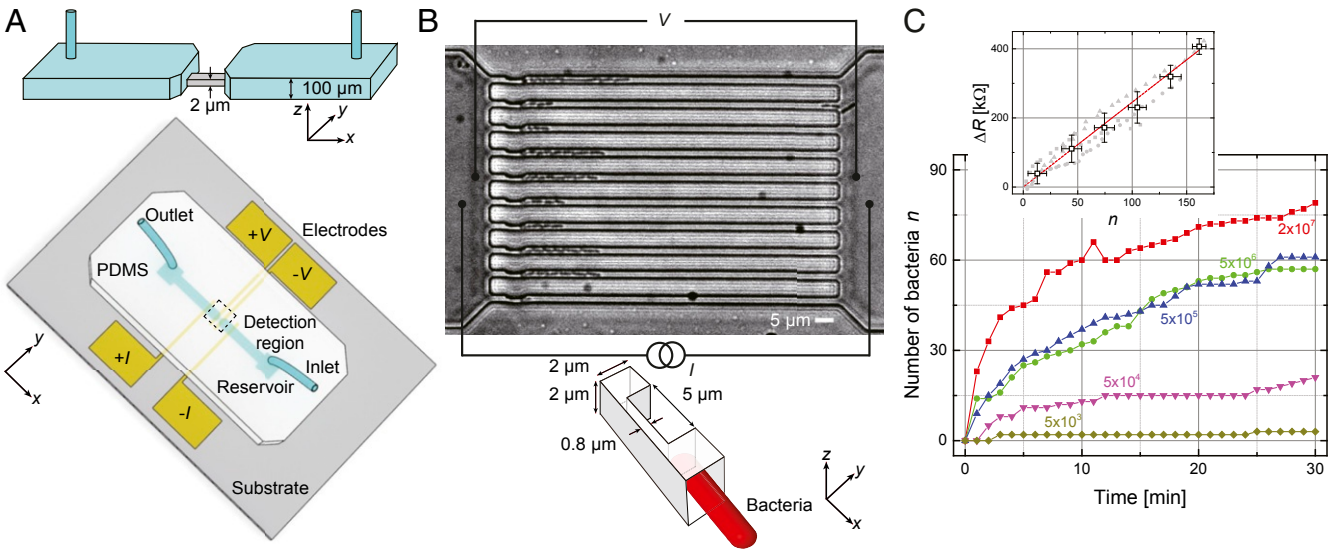

Fig. 1. Microfluidic device and its principle of operation. (*A*) Schematic of the device. The PDMS slab embedded with a two-layer microfluidic channel (*Inset*) is bonded onto a glass substrate with deposited thin film electrodes. At the center is the detection region, which features an array of 10 microchannels (2-μm height and 2-μm width) in parallel. These central microchannels are connected to two reservoirs via 100-μm-height macrochannels; the two reservoirs are connected to sample lines. (*B*) (*Top*) Microscope image (63×) of trapped bacteria (*K. pneumoniae*) in the microchannels. (Scale bar, 5 μm.) *Bottom* shows the constriction for capturing bacteria. A four-wire electrical resistance measurement is used. Growth and morphological changes of bacteria in the microchannel alter the effective electrical resistance of the microchannel. (*C*) Number of trapped bacteria (*K. pneumoniae*) in the microchannels as a function of sample loading time for cultures with different cell concentrations. *Inset* shows the electrical resistance change as a function of the number of bacteria in the microchannel from three nominally identical devices. The linear fit gives the resistance change per added bacterium of $\sim 2.5\ k\Omega$; the large data points correspond to binned average values.

such nonideal occurrences. First, the geometry ensures that the largest resistance signals come from the central detection region (*SI Appendix*, *Supplemental Materials and Methods*). Second, all bacteria inside the device, regardless of where they are, generate coherent electrical signals of cell growth or cell death. Third, any contaminants that partially block the device and do not change over time just result in time-independent background signals.

Electrical Monitoring of Bacterial Growth. We first perform an electrical measurement of bacteria growth. We record the device resistance $R(t)$ as a function of time. We then determine the normalized time-dependent resistance change defined as $\Delta R(t)/\Delta R(0) = (R(t) - R_{em})/(R(0) - R_{em})$, where $R(0)$ and R_{em}, respectively, are the device resistance right after loading ($t = 0$) and without bacteria (empty). From Fig. 1 *C*, *Inset*, we expect that $\Delta R(t)/\Delta R(0) \approx n(t)/n(0)$, where $n(t)$ is the number of bacteria in the microchannels. Fig. 2*A* shows the normalized resistance for motile *E. coli* as a function of time obtained in phosphate-buffered saline (PBS) at 37 °C and Luria–Bertani (LB) broth at 23 °C and 37 °C. After bacteria are loaded and during the measurement, $\Delta p \approx 0.5$ kPa is applied to maintain a constant flow of nutrients. Shown in Fig. 2 *A*, *Inset* are optical microscope images of the trapped *E. coli* taken at $t = 0,\ 20,\ 40$ min during the electrical measurement in LB broth at 37 °C (also see Movie S1).

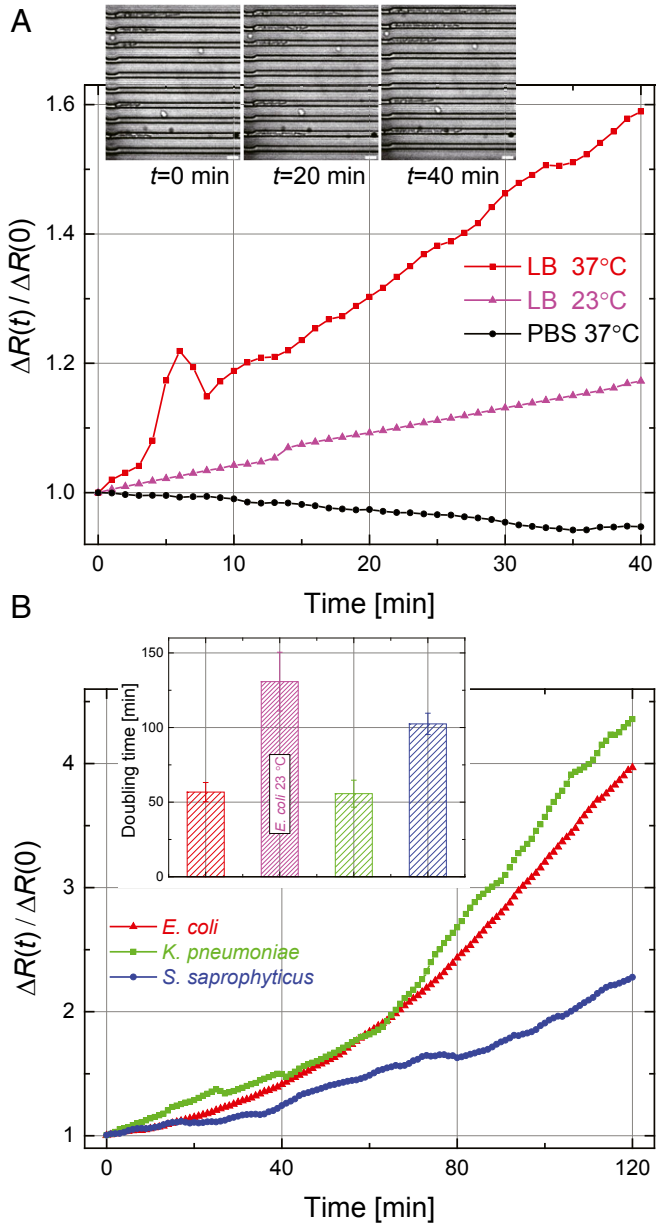

Fig. 2. Electrical detection of bacteria growth. (*A*) Growth curves for *E. coli* in PBS at 37 °C (black) and in LB broth at 23 °C (magenta) and 37 °C (red). *Inset* shows optical images of *E. coli* in the microchannels in LB broth at 37 °C at different points in time. (Scale bars, 5 μm.) (*B*) Growth curves for *E. coli* (red), *K. pneumoniae* (green), and *S. saprophyticus* (blue) at 37 °C in LB broth. Each data trace is the average of three independent experiments. (Error bars for the growth data are shown in Fig. 3.) *Inset* shows the doubling time. Error bars represent standard deviations.

Fig. 2*B* shows similar growth curves for gram-positive and gram-negative bacteria. *K. pneumoniae* and *S. saprophyticus* are nonmotile and are easily trapped in the microchannels by a pressure-driven flow; *E. coli* is motile but unlikely to reverse its direction and exit the tight microchannel once it enters. The electrical resistance changes are all close to exponentials: $\Delta R(t)/\Delta R(0) \approx n(t)/n(0) \approx e^{rt}$, with the growth rate r providing the doubling time $t_d = \ln 2/r$ for each strain. Fig. 2 *B*, *Inset* shows t_d values obtained from linear fits to the natural logarithms of the growth curves. The t_d we measure are longer than those reported in the literature (29–31), possibly due to the limited availability of nutrients in the microchannels (32).

Antibiotic Susceptibility Testing. We show, in Fig. 3, how our method and device can be used to determine the antibiotic susceptibility of bacteria rapidly and efficiently. We have tested bacterial response to two antibiotics with different action mechanisms: ampicillin, a β-lactam bactericidal antibiotic, and nalidixic acid, a bacteriostatic antibiotic at low concentration. Prior to the microfluidic experiments, the susceptibility of the bacteria and the minimum inhibitory concentration (MIC) values were determined from resazurin-based microdilution ASTs (*SI Appendix*, *Supplemental Materials and Methods* and Table S1). Each data trace in Fig. 3 was collected on a separate device. All of the results are presented in terms of the normalized resistance change, $\Delta R(t)/\Delta R(0)$, that is, the approximate number of bacteria in the microchannel as a function of time normalized by the initial number of bacteria. In each plot, the black curve shows the bacteria growth curve in LB broth with no antibiotics. The different curves show the results when bacteria are incubated in the presence of different concentrations of different antibiotics.

Fig. 3*A* shows the effect of two different antibiotics, ampicillin (red curves) and nalidixic acid (blue curves), on motile *E. coli*. (The black curve is the growth curve from Fig. 2*B*.) Our initial standardized ASTs confirm that *E. coli* is susceptible to both antibiotics at the indicated concentrations. In nalidixic acid, the measured resistance is approximately constant over time (Fig. 3*A*, blue curves), suggesting that the bacteria do not grow or change in any other way. In contrast, the electrical resistance in ampicillin (Fig. 3*A*, red curves) first increases but then takes a turn, staying constant or decreasing below the initial value. The behavior of the electrical resistance, without resorting to microscopy, is consistent with the fact that the cells elongate initially but cannot complete their division and eventually die. Fig. 3 *A*, *Inset* shows the growth rates r obtained from the normalized resistance curves. Here, we compute $d \ln [\Delta R(t)/\Delta R(0)]/dt$ within a sliding window of 20 min in order to reduce the numerical noise. The growth rates show that *E. coli* does not grow appreciably in either antibiotic at the noted concentrations, suggesting the strain is susceptible to both antibiotics. A straightforward metric for susceptibility can be obtained by averaging the growth rate in the second half of the test (i.e., last ~1 h). For this

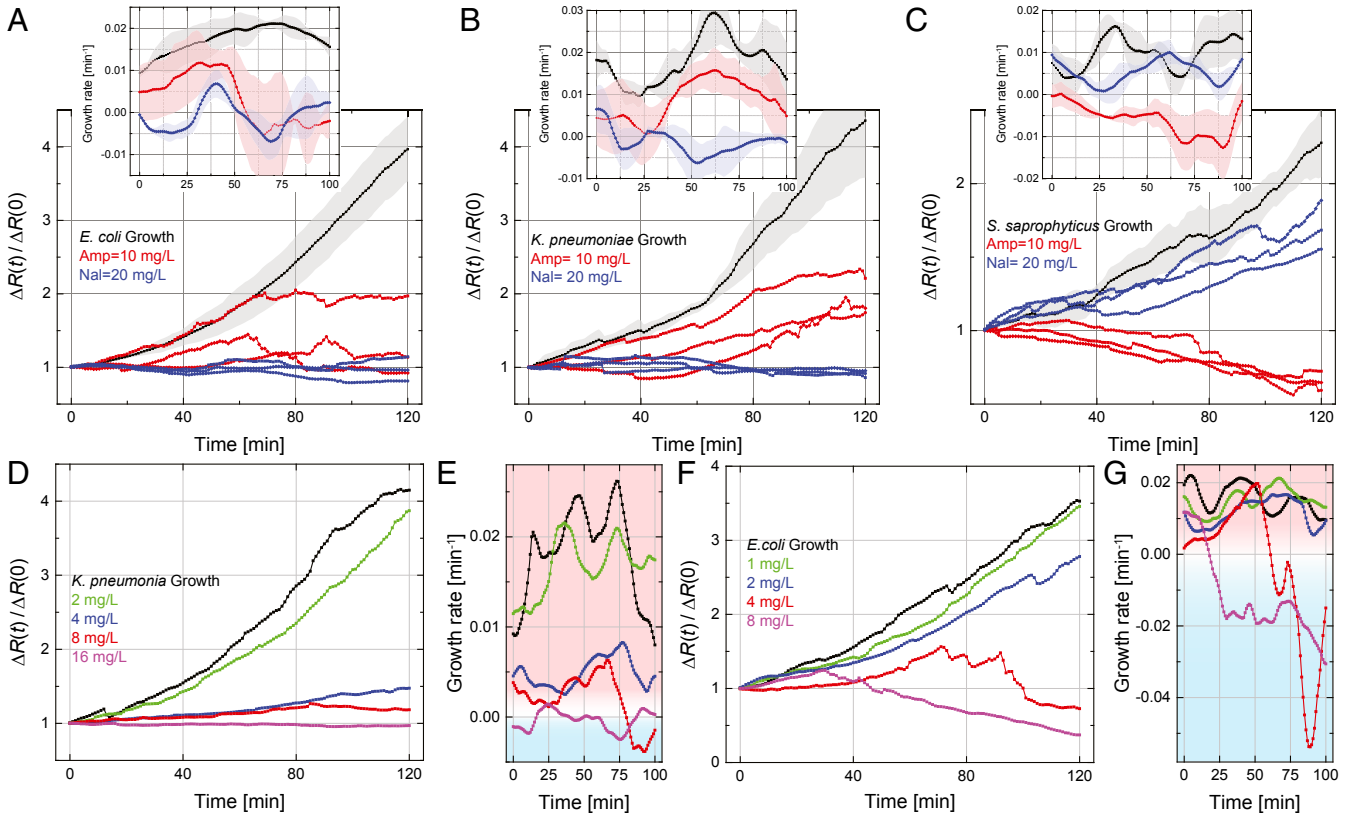

Fig. 3. (*A*–*C*) Electrical determination of the susceptibility of (*A*) *E. coli*, (*B*) *K. pneumoniae*, and (*C*) *S. saprophyticus* to ampicillin and nalidixic acid. Normalized resistance changes as a function of incubation time under different conditions are plotted for each strain. The black curve in each plot is the average growth curve in LB broth without antibiotics at 37 °C from Fig. 2*B*, with the shaded region showing the SD; the red and blue curves show the electrical signal in LB broth with added ampicillin (10 mg/L) and nalidixic acid (20 mg/L), respectively, at 37 °C. Each colored curve represents one independent experiment. *Insets* show the growth rate, $r \approx d\ln[\Delta R(t)/\Delta R(0)]/dt$, calculated from the normalized resistance changes in the main plots; each solid line and shaded region, respectively, show the average value and the SD from three experiments. (*D*–*G*) Determination of MIC. (*D*) Normalized resistance change for *K. pneumoniae* as a function of incubation time in human urine with different concentrations of nalidixic acid. (*E*) Growth rates for each curve in *D*. (*F*) Determination of ampicillin MIC for *E. coli* in human urine. (*G*) Growth rates for each curve in *F*.

dataset, we obtain $\bar{r}_G \approx 0.019\ \text{min}^{-1}$, $\bar{r}_{Amp} \approx -0.0037\ \text{min}^{-1}$, and $\bar{r}_{Nal} \approx -0.0017\ \text{min}^{-1}$, all averaged over three measurements. Thus, $\bar{r} \leq 0$ can be taken as an objective—albeit somewhat restrictive—condition for susceptibility. (In Fig. 4, we look at different aspects of the same data for differentiating between the action mechanisms of these antibiotics.)

For *K. pneumoniae* (Fig. 3*B*), the normalized resistance change in ampicillin (red curves) keeps increasing with incubation time, while that in nalidixic acid (blue curves) does not change at all. Fig. 3 *B*, *Inset* shows the growth rates as above. The data indicate that *K. pneumoniae* is resistant to ampicillin but susceptible to nalidixic acid at the indicated concentrations. We also observe that the growth rate of *K. pneumoniae* in ampicillin is lower than that with no drug. In the case of *S. saprophyticus* (Fig. 3*C*), the antibiotics cause different outcomes.

We next determine the MICs for nalidixic acid and ampicillin using our device and method. In an effort to show the clinical relevance, we perform the MIC experiments directly in bacteria-spiked human urine mixed with LB broth. MICs are determined within a 2-h time window. Fig. 3*D* shows the normalized resistance change as a function of time for *K. pneumoniae* in nalidixic acid at concentrations of 0, 2, 4, 8, and 16 mg/L. Increasing the concentration of nalidixic acid slows the growth down, eventually making the time derivative negative at a concentration of $\lesssim 16$ mg/L (Fig. 3*D*), suggesting that 16 mg/L can safely be taken as the MIC. The corresponding growth rates in Fig. 3*E* are negative at later times for the two highest antibiotic concentrations. From Fig. 3 *F* and *G*, we determine the MIC of ampicillin for a nonmotile strain of *E. coli*. The antibiotic becomes effective at a concentration of $\gtrsim 4$ mg/L but after ~ 80 min of exposure. These MIC values and our metric, $\bar{r}$, remain consistent with results obtained from standardized ASTs (*SI Appendix*, Tables S1 and S2).

Electrical Signatures of Antibiotic Mechanisms. We now take a more detailed look at the data presented in Fig. 3*A* for motile *E. coli* in two antibiotics, focusing on the short-time fluctuations of the resistance. We high-pass filter the time-dependent resistance data, rejecting drifts on time scales of $\gtrsim 100$ s. Fig. 4*A* shows samples of these resistance fluctuations as a function of time for ampicillin (red trace) and nalidixic acid (blue trace) from single 2-h measurements; the black data trace is collected in LB broth without bacteria. There appear to be more-frequent and higher-amplitude resistance fluctuations in ampicillin than in nalidixic acid, with the rms values being $\delta R_{amp} \approx 7.35\ \text{k}\Omega$ and $\delta R_{nal} \approx 0.93\ \text{k}\Omega$ during the 2-h measurement ($\delta R_{LB} \approx 0.52\ \text{k}\Omega$). Fig. 4 *A*, *Left Inset* shows the fluctuating signal in ampicillin on the time scale of a single fluctuation. Simultaneous time-lapse microscope images (Fig. 4 *A*, *Right Inset*) have allowed us to speculate about the source of this particular fluctuation in ampicillin. The images show that a bacterium in one of the 10 microchannels undergoes a rapid burst at roughly the same time as the disappearance of the sharp electrical peak. We speculate that the swelling of the bacteria increases the resistance before the

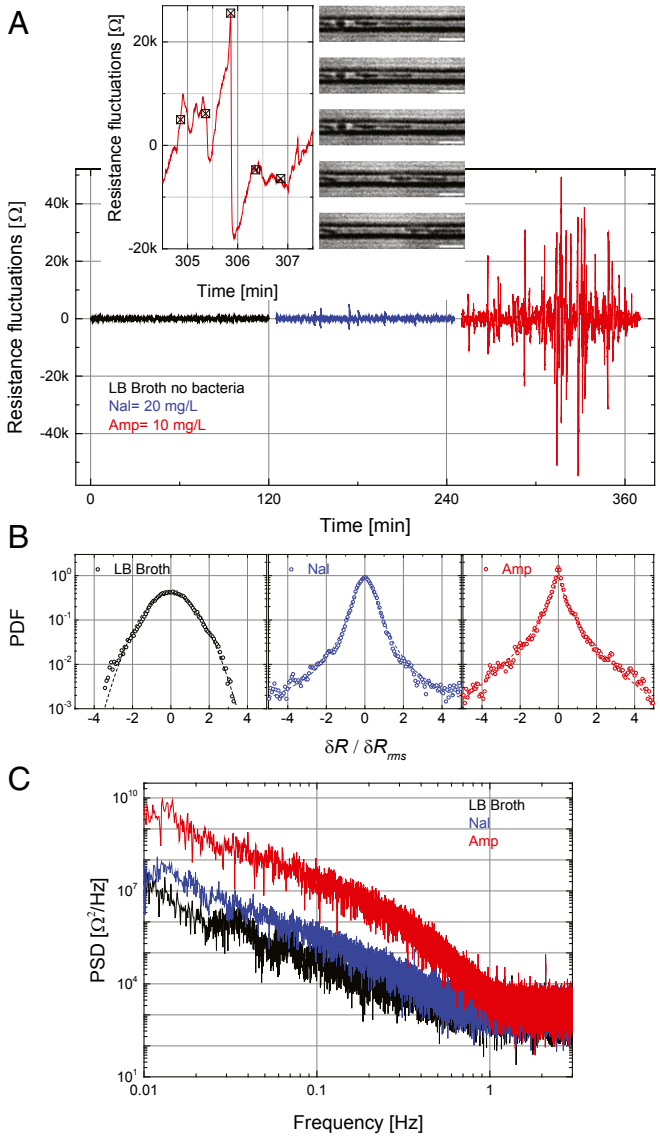

Fig. 4. Electrical signatures of action mechanisms of different antibiotics. (*A*) Time-dependent electrical resistance fluctuations of *E. coli* in ampicillin (red trace) and nalidixic acid (blue trace). The black curve shows the baseline fluctuations in pure LB broth with no trapped bacteria. *Insets* focus on a single peak along with microscope images recorded at the indicated instants. (Scale bars, 5 μm.) (*B*) Normalized PDFs plotted in units of the rms values of the fluctuations. The black dashed line is a Gaussian. The blue dashed line is a fit to $f(x) = A\exp[-\beta x^2/(1+|x|^{\nu})]$ with $A = 0.93$, $\beta = 4.65$, and $\nu = 1.78$. The red dashed line is a fit to $f(x) = A\exp(-\beta|x|^{\nu})$, with $A = 1.62$, $\beta = 2.85$, and $\nu = 0.55$. (*C*) The average PSDs of the signals.

burst, and the rapid burst gives rise to the sudden resistance drop (Movie S2). The microscope images show that bacteria to the right of the bursting bacterium are displaced even further and some residue remains in the microchannel after the burst. Bacteria in the other microchannels stay unchanged during this time interval. We have not noticed many similar cell bursting events in the 2-h time-lapse images of bacteria in nalidixic acid, which only inhibits cell division.

To provide more quantitative insight into antibiotic mechanisms, we calculate the probability density function (PDF) and the power spectral density (PSD) of the resistance fluctuations. For this, we use all three datasets for the same experiment, such as the ones in Fig. 4*A*. Fig. 4*B* shows the normalized PDFs in units of the rms fluctuation amplitude. The black data are the PDF of the background fluctuations collected in a device filled with just LB broth. These background fluctuations are, for the most part, Gaussian, with $\delta R_{bg} \approx 0.52$ kΩ. The blue data obtained from *E. coli* in nalidixic acid start to deviate from a Gaussian and can be fitted by a stretched exponential function. The red data in ampicillin with the sharp peaks strongly deviate from a Gaussian. Fig. 4*C* shows the average PSDs of these noise-like signals. The PSD of the signal in the bacteriostatic antibiotic (blue) is close to the PSD of the noise without bacteria. The added noise power due to the bactericidal effect (red) is at low frequencies in the range 0.01 Hz to 0.5 Hz, which is the high-frequency cut-off frequency in the measurement circuit. The $1/f$-like behavior of the PSD is probably due to the fact that the bursts take place on different time scales. We further compare the rms value of the fluctuations in ampicillin in the first half with that in the second half of the 2-h measurement, $\delta R^{(i)}_{amp} \approx 0.5\delta R^{(ii)}_{amp}$, indicating that ampicillin exhibits time-dependent bactericidal effect (33, 34).

Discussion

This work describes an electrical approach that determines bacterial susceptibility to antibiotics in a microfluidic device. In the simplest interpretation, the approach depends on the blockage of (quasi direct current) ionic current by intact bacteria (35). Upon further reflection, however, deeper questions emerge on how ionic current flows in pores and microchannels blocked by bacteria. Some of our microscope images suggest that, after cell lysis, the resistance tends to decrease even before the cell residue gets washed out by the liquid flow. We speculate that, once the cell wall and membrane lose their integrity, a bacterium may start to conduct ionic current at a higher rate through the cell body. In the case of rapid cell bursts, the residues are probably too small to significantly block the ionic current efficiently.

At the current stage of development, the entire setup consists of a basic Ohmmeter and a flow controller connected to the microfluidic device. Given that the approach does not require a high-resolution microscope, it could eventually be developed into a small and robust point-of-care platform, potentially usable in resource-limited settings. A few technical improvements are still needed: First, the sample loading process could be optimized. A higher applied pressure will allow the sample to flow faster and reduce the loading time (17). Currently, the pressure is limited by the bonding strength between PDMS and the substrate. A silicon-based device, while harder to fabricate, may solve this problem. Second, the electrical measurement can be multiplexed to increase the throughput, reduce the test time, or provide the susceptibility of bacteria to multiple antibiotics in parallel.

The fluctuations in the electrical signal due to antibiotic action are worth serious attention. The fluctuations in the bacteriostatic antibiotic are close to those in LB broth, with the slight increase in the rms amplitude possibly being due to the movements of the *E. coli* (36). The more interesting issue is the strong deviation of the fluctuations in the bactericidal antibiotic experiment from Gaussian statistics, approaching an exponential distribution. Apparently, the short, strong, and discrete peaks generated by the cell bursts are responsible for the observed behavior. This is reminiscent of wall turbulence, where strong and rare turbulent wall bursts completely dominate the velocity fluctuations in a similar manner. A focused parametric experimental study and a first-principles theory are needed for a more complete biophysical picture.

In the short term, our method is poised to have clinical relevance to UTI diagnosis and optimal treatment. While this work lays the foundation for an AST, further translational studies are needed for a clinical test. Patients with UTIs and possible comorbidities (e.g., diabetes, chronic renal disease) likely have

complex urine matrices that may not be directly usable in our device. However, uncomplicated UTI in otherwise healthy adult women is one of the most common UTI syndromes in outpatient medicine, and the need for rapid susceptibility testing to improve empirical therapy is increasing with more community-based gram-negative resistance (37). Polymicrobial UTIs, in which multipathogens with heterogeneous antibiotics response coexist, may require additional considerations.

Materials and Methods

Microfluidic Device. The microfluidic device consists of a PDMS microstructure (embedded with a two-layer microfluidic channel) that is permanently bonded with a glass substrate, which has metallic electrodes on it. We use standard soft lithography to fabricate the device. Details of the device fabrication process are described in *SI Appendix, Supplemental Materials and Methods*.

Bacterial Strains, Growth Media, and Antimicrobial Preparations. In this study, motile *E. coli* (ATCC 25922), *K. pneumoniae* (ATCC 13883), and *S. saprophyticus* (ATCC 15305) were purchased from American Type Culture Collection (ATCC), and nonmotile *E. coli* (JW 1908-1) was obtained from *E. coli* Genetic Stock Center. We used either LB broth (Sigma-Aldrich) or human urine (Lee Biosolutions) as growth media, depending on the experiment. The stock solutions of ampicillin and nalidixic acid were prepared using the methods provided by the supplier (Alfa Aesar). Details are provided in *SI Appendix, Supplemental Materials and Methods*.

Electrical Measurements and Data Acquisition. A lock-in amplifier (SR 830 DSP; Stanford Research Systems) is used to measure the resistances of the microchannels. The reference frequency and time constant are 10 Hz and 300 ms (bandwidth of $\sim$0.53 Hz), respectively. The output signals from the lock-in amplifier were recorded using a data acquisition card (NI 6221; National Instruments) through a LabVIEW (National Instruments) Virtual Instrument interface. The sampling rate for data collection is 6 Hz. The experimental data are analyzed using Origin (MicroCal Software) and MATLAB (MathWorks). Details of electrical measurements are given in *SI Appendix, Supplemental Materials and Methods*.

Image Collection. Images of the bacterial cells in the microchannels were obtained in an Axio observer inverted microscope (Carl Zeiss) using a 63$\times$ objective, an AxioCam 503 mono camera (Carl Zeiss), and ZEN image acquisition software (Carl Zeiss).

Data Availability. All data and procedures are included in the manuscript, *SI Appendix*, and Movies S1 and S2.

ACKNOWLEDGMENTS. This work was supported by NIH (1R21AI133264-01A1 and 1R03AI126168-01). We thank Joan O'Connor for assistance with sample preparation and resazurin-based broth microdilution ASTs and thank Deborah J. Stearns-Kurosawa and Victor Yakhot for discussions.

1. E. D. Brown, G. D. Wright, Antibacterial drug discovery in the resistance era. *Nature* **529**, 336–343 (2016).
2. J. M. Blair, M. A. Webber, A. J. Baylay, D. O. Ogbolu, L. J. Piddock, Molecular mechanisms of antibiotic resistance. *Nat. Rev. Microbiol.* **13**, 42–51 (2015).
3. R. A. Ataee, A. Mehrabi-Tavana, S. M. J. Hosseini, K. Moridi, M. G. Zadegan, A method for antibiotic susceptibility testing: Applicable and accurate. *Jundishapur J. Microbiol.* **5**, 341 (2012).
4. S. G. Jenkins, A. N. Schuetz, Current concepts in laboratory testing to guide antimicrobial therapy. *Mayo Clinic Proc.* **87**, 290–308 (2012).
5. A. van Belkum *et al.*, Developmental roadmap for antimicrobial susceptibility testing systems. *Nat. Rev. Microbiol.* **17**, 51–62 (2019).
6. M. Balouiri, M. Sadiki, S. K. Ibnsouda, Methods for in vitro evaluating antimicrobial activity: A review. *J. Pharm. Anal.* **6**, 71–79 (2016).
7. Z. A. Khan, M. F. Siddiqui, S. Park, Current and emerging methods of antibiotic susceptibility testing. *Diagnostics* **9**, 49 (2019).
8. C. Gonzalez-Gonzalez et al., Effect of physicians' attitudes and knowledge on the quality of antibiotic prescription: A cohort study. *PLoS One* **10**, e0141820 (2015).
9. H. L. Copp, D. J. Shapiro, A. L. Hersh, National ambulatory antibiotic prescribing patterns for pediatric urinary tract infection, 1998–2007. *Pediatrics* **127**, 1027–1033 (2011).
10. B. Li, T. J. Webster, Bacteria antibiotic resistance: New challenges and opportunities for implant-associated orthopedic infections. *J. Orthop. Res.* **36**, 22–32 (2018).
11. G. Rajivgandhi, M. Maruthupandy, G. Ramachandran, M. Priyanga, N. Manoharan, Detection of ESBL genes from ciprofloxacin resistant Gram negative bacteria isolated from urinary tract infections (UTIs). *Front. Lab. Med.* **2**, 5–13 (2018).
12. D. Hughes, D. I. Andersson, Environmental and genetic modulation of the phenotypic expression of antibiotic resistance. *FEMS Microbiol. Rev.* **41**, 374–391 (2017).
13. J. Dai, M. Hamon, S. Jambovane, Microfluidics for antibiotic susceptibility and toxicity testing. *Bioengineering* **3**, 25 (2016).
14. W. Kang, S. Sarkar, Z. S. Lin, S. McKenney, T. Konry, Ultrafast parallelized microfluidic platform for antimicrobial susceptibility testing of Gram positive and negative bacteria. *Anal. Chem.* **91**, 6242–6249 (2019).
15. J. Q. Boedicker, L. Li, T. R. Kline, R. F. Ismagilov, Detecting bacteria and determining their susceptibility to antibiotics by stochastic confinement in nanoliter droplets using plug-based microfluidics. *Lab Chip* **8**, 1265–1272 (2008).
16. J. C. Wang, S. W. Chi, T. H. Yang, H. S. Chuang, Label-free monitoring of microorganisms and their responses to antibiotics based on self-powered microbead sensors. *ACS Sens.* **3**, 2182–2190 (2018).
17. Ö. Baltekin, A. Boucharin, E. Tano, D. I. Andersson, J. Elf, Antibiotic susceptibility testing in less than 30 min using direct single-cell imaging. *Proc. Natl. Acad. Sci. U.S.A.* **114**, 9170–9175 (2017).
18. H. Li *et al.*, Adaptable microfluidic system for single-cell pathogen classification and antimicrobial susceptibility testing. *Proc. Natl. Acad. Sci. U.S.A.* **116**, 10270–10279 (2019).
19. M. S. Mannoor, S. Zhang, A. J. Link, M. C. McAlpine, Electrical detection of pathogenic bacteria via immobilized antimicrobial peptides. *Proc. Natl. Acad. Sci. U.S.A.* **107**, 19207–19212 (2010).
20. Q. Chen *et al.*, Fast and sensitive detection of foodborne pathogen using electrochemical impedance analysis, urease catalysis and microfluidics. *Biosens. Bioelectron.* **86**, 770–776 (2016).
21. J. D. Besant, E. H. Sargent, S. O. Kelley, Rapid electrochemical phenotypic profiling of antibiotic-resistant bacteria. *Lab Chip* **15**, 2799–2807 (2015).
22. P. Stupar *et al.*, Nanomechanical sensor applied to blood culture pellets: A fast approach to determine the antibiotic susceptibility against agents of bloodstream infections. *Clin. Microbiol. Infect.* **23**, 400–405 (2017).
23. B. Behera *et al.*, Emerging technologies for antibiotic susceptibility testing. *Biosens. Bioelectron.* **142**, 111552 (2019).
24. L. Yang, R. Bashir, Electrical/electrochemical impedance for rapid detection of foodborne pathogenic bacteria. *Biotechnol. Adv.* **26**, 135–150 (2008).
25. J. Choi *et al.*, A rapid antimicrobial susceptibility test based on single-cell morphological analysis. *Sci. Transl. Med.* **6**, 267ra174 (2014).
26. G. Pitruzzello *et al.*, Multiparameter antibiotic resistance detection based on hydrodynamic trapping of individual *E. coli*. *Lab Chip* **19**, 1417–1426 (2019).
27. Z. A. Khan, M. F. Siddiqui, S. Park, Progress in antibiotic susceptibility tests: A comparative review with special emphasis on microfluidic methods. *Biotechnol. Lett.* **41**, 221–230 (2019).
28. B. L. Duell *et al.*, Innate transcriptional networks activated in bladder in response to uropathogenic escherichia coli drive diverse biological pathways and rapid synthesis of IL-10 for defense against bacterial urinary tract infection. *J. Immunol.* **188**, 781–792 (2012).
29. E. Galli, C. Midonet, E. Paly, F. X. Barre, Fast growth conditions uncouple the final stages of chromosome segregation and cell division in *Escherichia coli*. *PLoS Genet.* **13**, e1006702 (2017).
30. M. Regué *et al.*, A gene, uge, is essential for *Klebsiella pneumoniae* virulence. *Infect. Immun.* **72**, 54–61 (2004).
31. R. Almeida, J. Jorgensen, Comparison of adherence and urine growth rate properties of *Staphylococcus saprophyticus* and *Staphylococcus epidermidis*. *Eur. J. Clin. Microbiol.* **3**, 542–545 (1984).
32. D. Yang, A. D. Jennings, E. Borrego, S. T. Retterer, J. Männik, Analysis of factors limiting bacterial growth in PDMS mother machine devices. *Front. Microbiol.* **9**, 871 (2018).
33. M. E. Levison, J. H. Levison, Pharmacokinetics and pharmacodynamics of antibacterial agents. *Infect. Dis. Clini.* **23**, 791–815 (2009).
34. P. Midolo, J. Turnidge, W. Munckhof, Is bactericidal activity of amoxicillin against Helicobacter pylori concentration dependent?*Antimicrob. Agents Chemother.* **40**, 1327 (1996).
35. M. Tsutsui *et al.*, Identification of individual bacterial cells through the intermolecular interactions with peptide-functionalized solid-state pores. *Anal. Chem.* **90**, 1511–1515 (2018).
36. V. Kara *et al.*, Microfluidic detection of movements of *Escherichia coli* for rapid antibiotic susceptibility testing. *Lab Chip* **18**, 743–753 (2018).
37. D. A. Talan *et al.*, Fluoroquinolone-resistant and extended-spectrum β-lactamase–producing Escherichia coli infections in patients with pyelonephritis, United States. *Emerg. Infect. Dis.* **22**, 1594 (2016).